Dalton Transactions

ROYAL SOCIETY OF CHEMISTRY

PAPER

View Article Online
View Journal | View Issue

Check for updates

Cite this: *Dalton Trans.*, 2025, **54**, 4599

The role of defect-modulated HKUST-1 MOF nodes in non-oxidative ethanol dehydrogenation: an observed phenomenon of catalyst transfiguration†

Anjali Ganai and Pranab Sarkar *

Received 26th November 2024,
Accepted 4th February 2025

DOI: 10.1039/d4dt03300k

rsc.li/dalton

Bioethanol production from agricultural residues has emerged as an important process of biomass valorization. The production of acetaldehyde from bioethanol has also started gaining ground. Since Cu-based catalysts are well-known for their ability to catalyse ethanol dehydrogenation, we have used a defect-modulated Cu-based metal–organic framework (MOF), HKUST-1, for obtaining mechanistic insights into the process. Defect-modulation in the form of a missing linker creates an easily accessible dual-atom site which can simultaneously participate in catalysing the reaction. Although ethanol dehydrogenation to ethylene competes with acetaldehyde production over both the defective HKUST-1(H) and HKUST-1(OH) MOF nodes, acetaldehyde formation occurs selectively. However, HKUST-1(OH) could not be regenerated at the end of the acetaldehyde formation pathway; HKUST-1(OH) ultimately transformed to HKUST-1(H) at the end of the cycle. This led to the introduction of the term 'catalyst transfiguration' where the catalyst, although transfigured, retains its ability to catalyse the reaction. Since, the HKUST-1(H) MOF node has the ability to selectively transform ethanol to acetaldehyde, we can safely conclude that the use of HKUST-1 (OH) will not cause acetaldehyde formation to come to a halt and the reaction can go on beyond the first catalytic cycle. Thus, both the defective MOF nodes can selectively transform ethanol to acetaldehyde.

Published on 17 February 2025. Downloaded on 3/19/2026 2:11:47 PM.

1. Introduction

The economic growth of a country largely depends on its industrial growth and development which causes significant utilization of conventional energy resources. This further aggravates the already existing environmental concern of global warming and greenhouse gas emissions. Policy-makers are now propagating the idea of a green economy since it maintains environmental sustainability while allowing the economic sector to flourish. An important step towards sustainability is to look for sustainable resources.[1–4] One such sustainable resource is biomass. Biomass appears to be an alternative to fossil fuels and also has the potential to produce several by-products.[5–7] Bioethanol production from agricultural residues has emerged as an important process of biomass valorization. Hence, the production of platform molecules from bioethanol has also started gaining ground.[8] One such platform molecule is acetaldehyde, which is known to produce a number of value added chemicals.

The typical process of acetaldehyde synthesis occurs *via* the Wacker process which involves oxidation of ethylene over a Pd/Cu catalyst. Since ethylene is obtained from steam cracking of petroleum hydrocarbons, Wackers process does not appear to be eco-friendly. Hence, conversion of bioethanol to acetaldehyde has emerged as an elegant process. Dehydrogenation of ethanol to acetaldehyde can occur *via* both an oxidative and non-oxidative pathway. Acetaldehyde production *via* an oxidative pathway involves the release of water which complicates product separation. Whereas, ethanol dehydrogenation *via* non-oxidative pathway involves the production of hydrogen instead of water and hence, simplifies product extraction. Hence, non-oxidative dehydrogenation of ethanol to acetaldehyde also provides an efficient route to the production of hydrogen, a clean renewable energy carrier, from waste biomass inputs.

Supported metal-nanoparticles have been extensively studied for ethanol dehydrogenation reaction where the nature of support material, the size of the nanoparticles and the presence of dopants have shown to have an influence on the catalytic activity.[9,10] Apart from utilizing Cu-nanoparticles, efforts have also been directed towards utilizing Zn-sites for ethanol dehydrogenation to acetaldehyde. A few examples include ZnO–CoO/Al_2O_3 nanoparticles, Cu/$ZnAl_2O_4$ catalyst and zeolites involving ZnO/silicalite-1 and ZnO/NaZSM-5.[11–14] Only a

Department of Chemistry, Visva-Bharati University, Santiniketan 731235, India.
E-mail: pranab.sarkar@visva-bharati.ac.in

† Electronic supplementary information (ESI) available: Details of microkinetic modeling analysis and optimized structures. See DOI: https://doi.org/10.1039/d4dt03300k

Published on 17 February 2025. Downloaded on 3/19/2026 2:11:47 PM.

few reports exist on utilizing metal–organic frameworks for catalysing the ethanol dehydrogenation reaction.[15,16]

Based on the findings from previous studies, copper catalysts have been observed to be efficient in catalysing the non-oxidative ethanol dehydrogenation reaction.[17–21] However, catalyst deactivation due to agglomeration of Cu-particles adversely affects the catalytic efficiency.[22–24] In order to overcome this problem, Giannakakis *et al.* have implemented an active site isolation strategy in the form of single-atom alloys to enhance the catalytic performance in non-oxidative ethanol dehydrogenation.[19,25] A recent study on ethanol dehydrogenation by Tang *et al.* pointed out that Cu-clusters are more efficient than single atom catalysts in catalysing acetaldehyde formation.[18] Since dual-atom catalysts (DACs) act as a bridge between single-atom catalysts and metal/alloy nanoparticles,[26] we hypothesise that DACs can provide the advantage of efficient atom utilization along with the synergistic effects arising from interaction between adjacent active sites.[27]

Metal–organic frameworks (MOFs) are porous networked structures composed of metal nodes connected by organic linkers. Since the metal centres present at the MOF nodes are isolated, they can serve as an active site for catalytic reactions. Hence, the risk of catalyst deactivation by agglomeration is negligible. In order to elucidate this idea, we have chosen a Cu-based MOF, HKUST-1, for our present study. The local environment presented by the MOF node in HKUST-1 is similar to the one observed in dual-atom catalysts. The presence of adjacent metal-sites in HKUST-1 attracts our attention since it can enhance MOF functionality when coupled with a missing linker defect.

HKUST-1, a copper-paddlewheel-based MOF, is composed of dimeric cupric carboxylate units connected with benzene-1,3,5-tricarboxylate to form a three-dimensional cubic crystal. The coordination polyhedron around each Cu(II)-centre is a tetragonal pyramid where the carboxylate oxygens form the base, and the oxygen atom of the coordinated water molecule occupies the top of the pyramid.[28,29] Thermal activation of this hydrated MOF causes the loss of water molecules which in turn results in the formation of coordinatively unsaturated sites (CUS).[30] A small portion of dehydrated HKUST-1 MOF is presented in Fig. 1(a). An enlarged view of the MOF node is presented in Fig. 1(b). These coordinatively unsaturated Cu^{2+} sites at the Cu–Cu node of HKUST-1 make it an attractive choice for gas-separation and catalytic processes.[31–33] However, the steric hindrance induced by the organic linker, isolates one Cu^{2+} centre from the other and hence their simultaneous involvement in catalysing a reaction is hindered. Defect modulation in MOFs has been a long known procedure for creating open MOF structures that enable enhanced MOF functionalities.[34–36] Defect modulation in HKUST-1 has been observed either in the form of a missing linker defect or in the form of a missing paddlewheel defect.[37] Loss of a linker in HKUST-1 results in the formation of an easily accessible dual-atom site which might result in enhanced catalytic activity.

Now, selectivity of a reaction is an important aspect of catalytic efficiency and reactant utilization. Previous studies on non-oxidative ethanol dehydrogenation have already pointed out a competing reaction along this pathway – ethanol transformation to ethylene.[38,39] Hence, a catalyst that can selectively favour acetaldehyde formation over ethylene synthesis would be preferred.

With the intention of exploring reaction selectivity, we carry out a computational investigation on the role of a defect-modulated dual-atom catalyst in catalysing the non-oxidative ethanol dehydrogenation reaction. In the present study, we have computationally modelled missing linker defects in HKUST-1 as: (1) HKUST-1(H) where the organic linker has been replaced by a hydride species (Fig. 1(c)); and (2) HKUST-1 (OH) where the organic linker has been replaced by a hydroxyl group (Fig. 1(d)). Metal-hydrides incorporated onto defective HKUST-1 are not uncommon[40] and have been experimentally synthesised *via* thermal activation of HKUST-1 in an atmosphere of hydrogen.[41] The defect modulated HKUST-1(OH) MOF nodes have also been computationally investigated by Xue *et al.* for CO oxidation.[42]

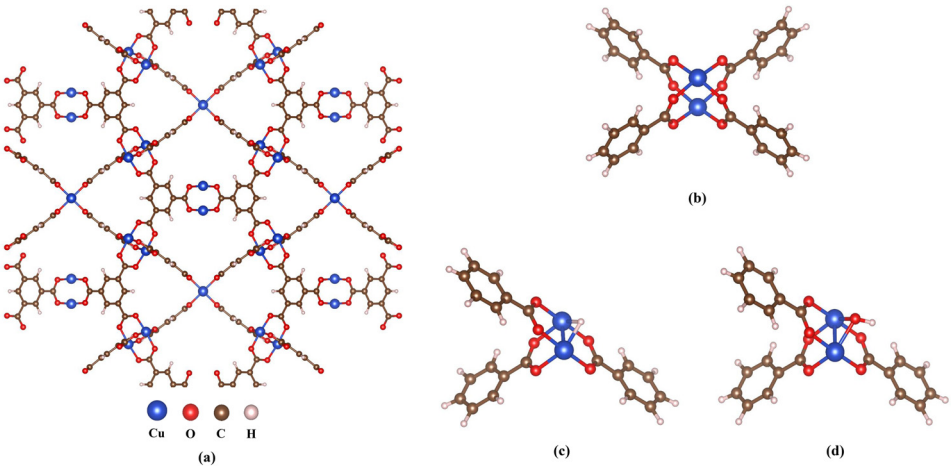

Fig. 1 (a) A small portion of dehydrated HKUST-1, (b) copper-paddlewheel node structure of dehydrated HKUST-1, (c) DFT cluster model of HKUST-1(H) and (d) DFT cluster model of HKUST-1(OH).

 This journal is © The Royal Society of Chemistry 2025

Published on 17 February 2025. Downloaded on 3/19/2026 2:11:47 PM.

Ethanol dehydrogenation to ethylene was found to compete with acetaldehyde production over both HKUST-1(H) and HKUST-1(OH). It was found that acetaldehyde formation was preferred over ethylene formation over both the defective MOF nodes. However, HKUST-1(OH) could not be regenerated at the end of the acetaldehyde formation pathway; HKUST-1(OH) was ultimately transformed to HKUST-1(H) at the end of the cycle. Since the HKUST-1(H) MOF node holds the ability to selectively transform ethanol to acetaldehyde, we name this phenomenon 'catalyst transfiguration' where the catalyst (*i.e.* HKUST-1(OH)), although transfigured (to HKUST-1(H)), retains its ability to catalyse the reaction. Hence, the use of HKUST-1(OH) will not cause acetaldehyde formation to come to a halt and the reaction can go on beyond the first catalytic cycle.

2. Computational details

Since the unit cell of HKUST-1 consists of a large number of atoms and we are primarily concerned with the activity of the Cu-paddlewheel unit, we cut out a cluster model as represented in Fig. 1(c). The organic linkers were truncated as a benzoate group. Hydrogen atoms were used to saturate the dangling bonds resulting from truncation.[43,44] The benzene rings were frozen to mimic the rigidity of a MOF framework. Hashem *et al.* have used a similar cluster model in their computational study on the ethylene dimerization reaction.[40] The confinement effects due to MOF framework were found to be negligible and hence, we can conclude that this cluster model accurately represents the structural features of HKUST-1.

The Gaussian 16 package[45] was used to perform all the DFT calculations. The M06-L functional has been recommended for transition metal and organometallic systems and hence, the computated cluster models were optimized using the M06-L functional with an ultrafine grid.[40] Geometry optimization and frequency calculations were carried out at the M06-L/GENECP level with a def2-SVP basis set for C, H, and O atoms while the Cu atoms were treated with the SDD basis set with the corresponding effective core potential (ECP) to account for any relativistic effect. Any minima along the potential energy surface was confirmed by the presence of zero imaginary frequency, while transition states were confirmed by the presence of one and only one, imaginary frequency. Intrinsic reaction coordinate (IRC) calculations were performed to confirm that we obtained the desired transition state. Single point energies were further calculated at the M06-L/def2-TZVP level. The presence of two Cu^{2+} centres introduces the possibility of antiferromagnetic behaviour and hence both the singlet and triplet multiplicities were considered to obtain spin crossing phenomena. The reaction profiles presented in the current work include both the singlet and triplet states in order to account for spin inversion processes along the lowest energy mechanistic pathway.[42] In the present study, the reported energies are Gibbs energies at 453.15 K. The reaction condition chosen here is in accordance with the experimental study reported by Patel *et al.*[19] on non-oxidative ethanol dehydrogenation over single-atom alloys. The following equations were used to calculate the forward and backward rate constants (in s^{-1}) for each elementary step involved in the catalytic pathway.

$$k_{\mathrm{for,i}} = \frac{k_{\mathrm{B}}T}{h} e^{\frac{-\Delta G^{\ddagger}_{\mathrm{for,i}}}{RT}} \tag{1}$$

$$k_{\mathrm{rev,i}} = \frac{k_{\mathrm{B}}T}{h} e^{\frac{-\Delta G^{\ddagger}_{\mathrm{rev,i}}}{RT}} \tag{2}$$

For any elementary reaction i, the equilibrium constant is defined as

$$K_{\mathrm{eq,i}} = \frac{k_{\mathrm{for,i}}}{k_{\mathrm{rev,i}}} = e^{\frac{-\left(\Delta G^{\ddagger}_{\mathrm{for,i}} - \Delta G^{\ddagger}_{\mathrm{rev,i}}\right)}{RT}} \tag{3}$$

where $k_{\mathrm{for,i}}$ and $k_{\mathrm{rev,i}}$ represent the forward and reverse rate constants for each elementary step i, $\Delta G^{\ddagger}_{\mathrm{for,i}}$ and $\Delta G^{\ddagger}_{\mathrm{rev,i}}$ represent the forward and reverse activation free energies for each elementary step i, $K_{\mathrm{eq,i}}$ is the equilibrium constant for each elementary step i, k_{B} is the Boltzmann's constant, T is the temperature in Kelvin, R is the gas constant and h is Planck's constant.

3. Results and discussion

3.1. Defect-free HKUST-1 MOF node

The defect-free node of HKUST-1 (Fig. 1(b)) possesses one CUS per Cu^{2+} centre, thus providing two CUS per HKUST-1 node. Although the individual CUS provides a site for reactant adsorption, reactant transformation to product is hindered due to the absence of a nearby vacant site. Moreover, the steric hindrance induced by the organic linker makes the simultaneous utilization of both CUS impossible. We thus conclude that the defect-free HKUST-1 node is unsuitable for non-oxidative ethanol dehydrogenation. Defect modulation in the form of missing linker defects makes the structure more open, allowing reactant adsorption followed by their transformation to products *via* simultaneous utilization of CUS. This is supported by the computational studies on (1) CO oxidation over defective HKUST-1 by Xue *et al.*[42] and (2) ethylene dimerization over defective HKUST-1 by Hashem *et al.*[40] With this idea in mind, we proceed with the defective HKUST-1(H) MOF node for ethanol dehydrogenation.

3.2. Defective HKUST-1(H) MOF node

3.2.1. Ethanol dehydrogenation to acetaldehyde. The schematic diagram of the proposed catalytic pathways is presented in Fig. 2. The resting state of the catalyst is represented as 1-H. The hydride species in the resting state of the catalyst occupies a bridging position between the dimeric Cu centres (Fig. 1(c)). This is in accordance with what has been reported by Hashem *et al.* in their computational study on ethylene dimerization.[40] Ethanol dehydrogenation on the defective HKUST-1(H) MOF node begins with the adsorption of ethanol at one Cu-centre. The adsorbed molecule then undergoes O–H bond dis-

Published on 17 February 2025. Downloaded on 3/19/2026 2:11:47 PM.

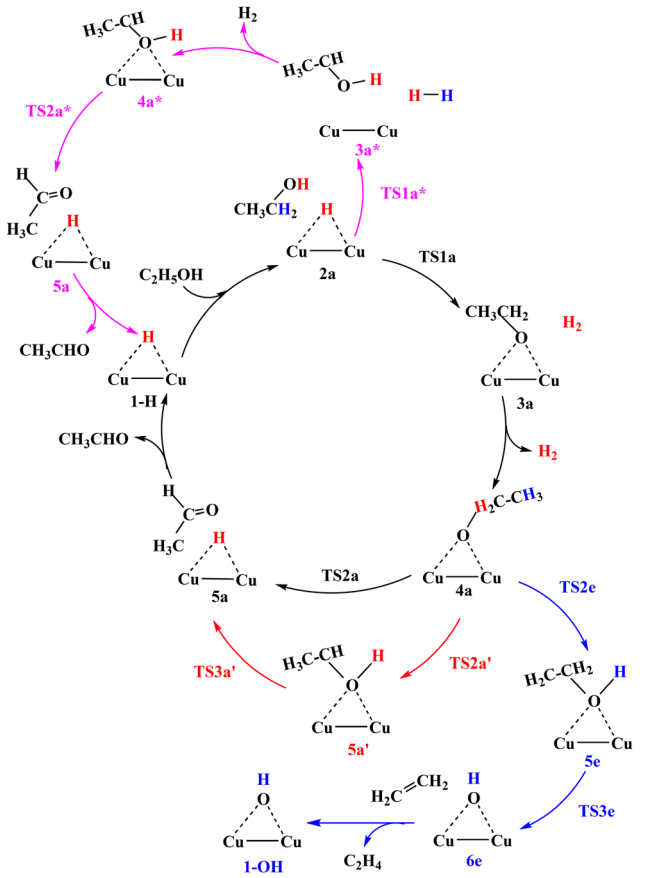

Fig. 2 Schematic diagram for the proposed pathways of ethanol dehydrogenation to acetaldehyde and ethanol dehydration to ethylene over the defective HKUST-1(H) MOF node. Only the Cu active sites have been shown for clarity. The cycle corresponding to black arrows represent path-a, that corresponding to red arrows represent path-b while that corresponding to pink arrows represent path-c.

sociation *via* TS1a which results in the formation of a hydrogen molecule and ethoxy intermediate. Dissociation of an α C–H bond of the ethoxy intermediate results in the formation of acetaldehyde. The transfer of the H-atom to the Cu-centre can either occur directly *via* TS2a or occur *via* intermediate **5a′** where the H-atom is first transferred to the O-atom before being transferred to the Cu-centre. We refer to the former pathway as 'path-a' and the latter pathway as 'path-b'. In addition to the two pathways observed over HKUST-1(H), another pathway for acetaldehyde formation was also observed. We refer to this pathway as 'path-c'. The pathway begins with the adsorption of an ethanol molecule followed by the cleavage of an α C–H bond which results in the formation of hydroxyethyl intermediate (**4a***) and a H_2 molecule. O–H bond dissociation subsequently follows to regenerate the catalyst along with the production of an acetaldehyde molecule (Fig. 2). The transformation can be represented as follows: HKUST-1(H) + CH_3CH_2OH → HKUST-1(H) + CH_3CHO + H_2.

The reaction profiles for ethanol transformation to acetaldehyde and ethylene over HKUST-1(H) are presented in Fig. 3.

Using the reaction profile shown in Fig. 3, we then performed microkinetic modeling (MKM) analysis to gain significant insight into the catalytic process.[42] The elementary steps involved in MKM analysis along with the DFT calculated activation barriers, forward and reverse rate constants and the equilibrium constants, have been summarized in Table 1. The rate constants were calculated at the experimental condition of 453.15 K with the partial pressures for ethanol, hydrogen and acetaldehyde being 0.05 kPa, 10^{-6} kPa and 10^{-6} kPa, respectively.[19] The details regarding kinetic model construction are presented in the ESI.† The Sabatier rates for acetaldehyde formation are as follows:

$$\text{rate(path-a)} = \frac{k_{\text{for},3}K_{\text{eq},1}K_{\text{eq},2}\dfrac{p_{\text{ethanol}}}{p_{H_2}}}{1 + K_{\text{eq},1}p_{\text{ethanol}} + K_{\text{eq},1}K_{\text{eq},2}\dfrac{p_{\text{ethanol}}}{p_{H_2}}} \quad (4)$$

$$\text{rate(path-b)} = \frac{k_{\text{for},3}K_{\text{eq},1}K_{\text{eq},2}\dfrac{p_{\text{ethanol}}}{p_{H_2}}}{1 + K_{\text{eq},1}p_{\text{ethanol}} + K_{\text{eq},1}K_{\text{eq},2}\dfrac{p_{\text{ethanol}}}{p_{H_2}} + \dfrac{p_{\text{acetaldehyde}}}{K_{\text{eq},4}}} \quad (5)$$

$$\text{rate(path-c)} = \frac{k_{\text{for},2}K_{\text{eq},1}p_{\text{ethanol}}}{1 + K_{\text{eq},1}p_{\text{ethanol}} + \dfrac{p_{\text{acetaldehyde}}}{K_{\text{eq},3}}} \quad (6)$$

Absolute free energy values obtained from DFT calculations usually suffer from an uncertainty estimate of 20 kJ mol^{-1} which introduces an uncertainty factor of 10^{-4} for calculated rate constants.[42] Thus, it is very difficult to obtain accurate rate constant values from DFT calculation.[46,47] We, therefore, deal with relative rate constant values instead of absolute ones. The absolute rate constant values have been normalized against the smallest rate constant value of 1.649×10^{-14} s^{-1}. The calculated relative acetaldehyde formation rates for path-a, path-b and path-c are 3.59×10^{16} s^{-1}, 1 s^{-1} and 8.72×10^{7} s^{-1}, respectively (Table 2). This indicates that acetaldehyde formation *via* ethoxy intermediate (*i.e.* path-a) is favoured over the remaining two pathways.

3.2.2. Ethanol dehydrogenation to ethylene. Apart from the three pathways mentioned above, our study reveals another competing pathway along with the proposed pathway of ethanol dehydrogenation–ethanol dehydrogenation to ethylene. Starting from intermediate **4a** (in Fig. 2), dissociation of a C–H bond of the ethoxy methyl carbon results in the formation of ethylene which further desorbs to vacate the active site. Here, it is important to note that transformation of ethanol to ethylene over HKUST-1(H) does not regenerate the catalyst. HKUST-1(H) has been ultimately transformed into HKUST-1 (OH) at the end of the catalytic pathway. The transformation can be represented as follows: HKUST-1(H) + CH_3CH_2OH → HKUST-1(OH) + C_2H_4 + H_2.

We thus conclude, that ethylene formation over HKUST-1 (H) can subsequently poison the catalyst and hence, we would like to avoid this competing pathway. The reaction profile for

 This journal is © The Royal Society of Chemistry 2025

Published on 17 February 2025. Downloaded on 3/19/2026 2:11:47 PM.

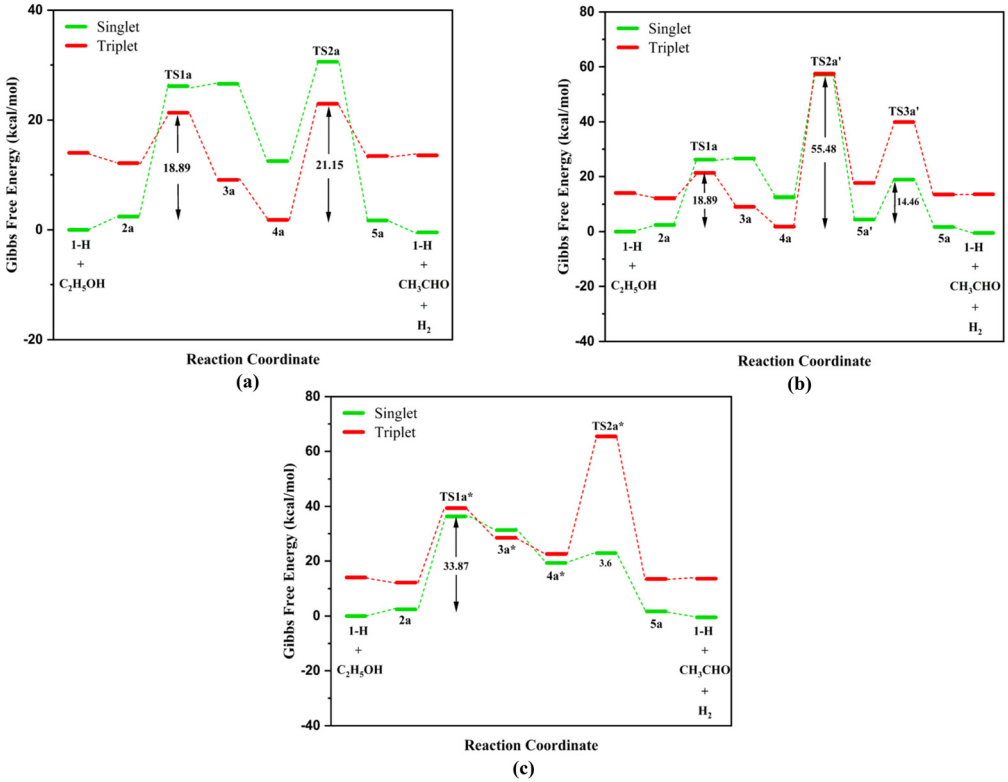

Fig. 3 The reaction profile of acetaldehyde formation from ethanol *via* (a) path-a, (b) path-b, and (c) path-c, over the defective HKUST-1(H) MOF node. All energies are reported relative to the separated state of catalyst and reactant.

Table 1 Summary of the forward $\Delta G^{\ddagger}_{\text{for,i}}$ and reverse $\Delta G^{\ddagger}_{\text{rev,i}}$ activation barriers in kcal mol^{-1}, the forward $k_{\text{for,i}}$ and reverse $k_{\text{rev,i}}$ rate constants in s^{-1} and the equilibrium constant $K_{\text{eq,i}}$ values for each elementary step i

Step i	Reaction	$\Delta G^{\ddagger}_{\text{for,i}}$	$\Delta G^{\ddagger}_{\text{rev,i}}$	$k_{\text{for,i}}$	$k_{\text{rev,i}}$	($K_{\text{eq,i}}$)
Path-a						
R1	$CH_3CH_2OH(g) + * \rightarrow *CH_3CH_2OH$	2.44	0	6.28×10^{11}	9.44×10^{12}	0.066
R2	$*CH_3CH_2OH + H \rightarrow *CH_3CH_2O + *H_2$	18.90	12.26	7.25×10^{3}	1.15×10^{7}	0.63×10^{-3}
R3	$*CH_3CH_2O + *H_2 \rightarrow *CH_3CH_2O + H_2(g) + *$	0	7.25	9.44×10^{12}	3.02×10^{9}	3.13×10^{3}
R4	$*CH_3CH_2O \rightarrow *CH_3CHO + H$	21.15	21.26	5.92×10^{2}	5.26×10^{2}	1.12
R5	$*CH_3CHO \rightarrow CH_3CHO\ (g) + *$	0	2.18	9.44×10^{12}	8.36×10^{11}	11.30
Path-b						
R1	$CH_3CH_2OH(g) + * \rightarrow *CH_3CH_2OH$	2.44	0	6.28×10^{11}	9.44×10^{12}	0.066
R2	$*CH_3CH_2OH + H \rightarrow *CH_3CH_2O + *H_2$	18.90	12.26	7.25×10^{3}	1.15×10^{7}	0.63×10^{-3}
R3	$*CH_3CH_2O + *H_2 \rightarrow *CH_3CH_2O + H_2(g) + *$	0	7.25	9.44×10^{12}	3.02×10^{9}	3.13×10^{3}
R4	$*CH_3CH_2O \rightarrow *CH_3CHOH$	55.48	52.87	1.65×10^{-14}	2.94×10^{-13}	5.6×10^{-2}
R5	$*CH_3CHOH \rightarrow *CH_3CHO + H$	14.46	17.16	9.98×10^{5}	4.99×10^{4}	19.97
R6	$*CH_3CHO \rightarrow CH_3CHO(g) + *$	0	2.18	9.44×10^{12}	8.36×10^{11}	11.30
Path-c						
R1	$CH_3CH_2OH(g) + * \rightarrow *CH_3CH_2OH$	2.44	0	6.28×10^{11}	9.44×10^{12}	0.066
R2	$*CH_3CH_2OH + H \rightarrow *CH_3CHOH + *H_2$	33.87	7.80	4.34×10^{-4}	1.63×10^{9}	2.66×10^{-13}
R3	$*CH_3CHOH + *H_2 \rightarrow *CH_3CHOH + H_2(g) + *$	0	9.23	9.44×10^{12}	3.34×10^{9}	2.83×10^{4}
R4	$*CH_3CHOH \rightarrow *CH_3CHO + H$	3.6	21.16	1.73×10^{11}	5.87×10^{2}	2.95×10^{8}
R5	$*CH_3CHO \rightarrow CH_3CHO(g) + *$	0	2.18	9.44×10^{12}	8.36×10^{11}	11.30

ethanol transformation to ethylene over HKUST-1(H) are presented in Fig. 4.

We now try to figure out the reaction selectivity using classical transition state theory (TST). A close inspection of the reaction profile shows that the rate determining step of acetaldehyde formation *via* path-a involves TS2a and that for ethylene synthesis involves TS2e. Hence, the overall free energy barrier $\Delta G^{\ddagger}_{\text{overall}}$ for each catalytic pathway comes out to be:

$$\Delta G^{\ddagger}_{\text{overall}}(\text{path-a}) = 22.98\ \text{kcal mol}^{-1} \quad (7)$$

$$\Delta G^{\ddagger}_{\text{overall}}(\text{path-ethylene}) = 51.23\ \text{kcal mol}^{-1} \quad (8)$$

Published on 17 February 2025. Downloaded on 3/19/2026 2:11:47 PM.

Table 2 Table summarizing the DFT-calculated rate-determining step, activation barrier for the rate limiting step $\Delta G^{\ddagger}$ (in kcal mol^{-1}) and the relative rate constant values

Pathway	Rate-determining step	$\Delta G^{\ddagger}$	Relative rate constant
Path-a	$*C_2H_5O \rightarrow CH_3CHO(g) + * + H$	21.15	3.59×10^{16}
Path-b	$*CH_3CH_2O \rightarrow *CH_3CHOH$	55.48	1
Path-c	$*CH_3CH_2OH + H \rightarrow *CH_3CHOH + H_2(g)$	33.87	8.72×10^{7}

The rate constants of the overall reactions derived using TST are: 77.48 s^{-1} for path-a and 1.83×10^{-12} s^{-1} for path-ethylene. This confirms that acetaldehyde formation *via* path-a occurs selectively over ethylene formation.

Considering that the defective HKUST-1(H) can catalyse acetaldehyde formation *via* path-a (involving an activation barrier of 21.15 kcal mol^{-1} for the rate limiting α-C–H bond dissociation step of the ethoxy intermediate), we now compare our results with the previously reported studies to figure out its catalytic efficiency. Ethanol dehydrogenation using NiAu-single-atom alloys have shown OH bond cleavage to be rate determining with an activation barrier of 27 kcal mol^{-1}.[25] Another study using NiCu-single-atom alloys also shows a similar barrier for the rate limiting α-C–H bond dissociation step.[19] A recent study on ethanol dehydrogenation using h-BN-supported Cu clusters shows the synergistic role of Cu^0 and Cu^+ sites in catalysing the reaction, and points out the formation of the H_2 molecule to be rate limiting with an activation barrier of 27.2 kcal mol^{-1}. We thus conclude, that defective HKUST-1(H) can effectively and selectively catalyse ethanol dehydrogenation to acetaldehyde.

Since catalytic transformation of ethanol to ethylene over the defective HKUST-1(H) MOF node could not regenerate the catalyst, this spurred our interest in studying the mechanistic pathway of ethanol dehydrogenation over the HKUST-1(OH) MOF node.

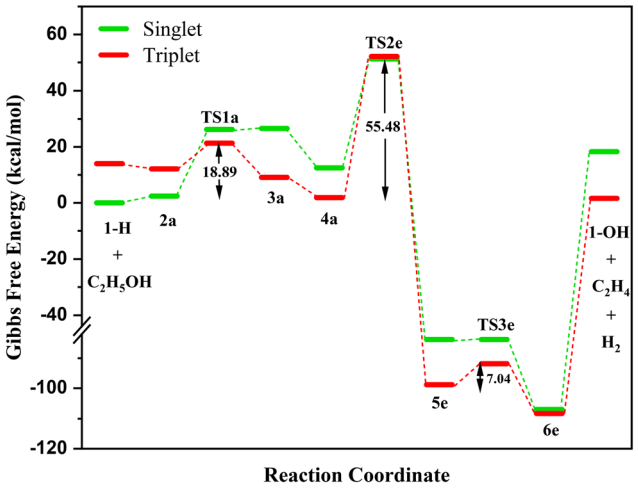

Fig. 4 The reaction profile of ethylene formation from ethanol over the defective HKUST-1(H) MOF node. All energies are reported relative to the separated state of catalyst and reactant.

3.3. Defective HKUST-1(OH) MOF node

Fig. 5 presents the schematic diagram for the catalytic pathway of acetaldehyde and ethylene formation from ethanol. The resting state of the catalyst has been represented as 1-OH. The hydroxyl group in the resting state of the catalyst occupies a bridging position between the dimeric Cu centres (Fig. 1(d)). The mechanistic pathway of acetaldehyde formation over HKUST-1(OH) is similar to that over HKUST-1(H) (Fig. 2). The only difference being that acetaldehyde formation over HKUST-1(H) resulted in the release of a hydrogen molecule whereas, acetaldehyde formation over HKUST-1(OH) results in the release of a water molecule. However, a pathway similar to path-c was not observed for acetaldehyde formation over HKUST-1(OH). Here, it is important to note that transformation of ethanol to acetaldehyde over HKUST-1(OH) does not regenerate the catalyst. HKUST-1(OH) has been ultimately transformed into HKUST-1(H) at the end of the catalytic pathway. The transformation can be represented as follows: HKUST-1(OH) + CH_3CH_2OH → HKUST-1(H) + $CH_3CHO + H_2O$.

Again, a competing pathway for ethylene formation was observed along with the proposed pathway of acetaldehyde formation. Starting from intermediate **4a**, dissociation of a C–H bond of the ethoxy methyl carbon results in the formation of ethylene which further desorbs to regenerate the catalyst (Fig. 5). The transformation can be represented as follows: HKUST-1(OH) + CH_3CH_2OH → HKUST-1(OH) + $C_2H_4 + H_2O$.

The reaction profiles for ethanol transformation to acetaldehyde and ethylene over HKUST-1(OH) are presented in Fig. 6.

A close inspection of the reaction profile shows that the rate determining step of path-a and path-b of acetaldehyde synthesis involves TS2a and TS2a′, respectively, and that for ethylene synthesis it involves TS2e. Hence, it becomes clear that acetaldehyde formation *via* path-a is preferred over the other two existing pathways. Even though, catalytic transformation of ethanol to acetaldehyde over defective-HKUST-1(OH) does not regenerate the catalyst, this pathway is preferred over ethylene synthesis.

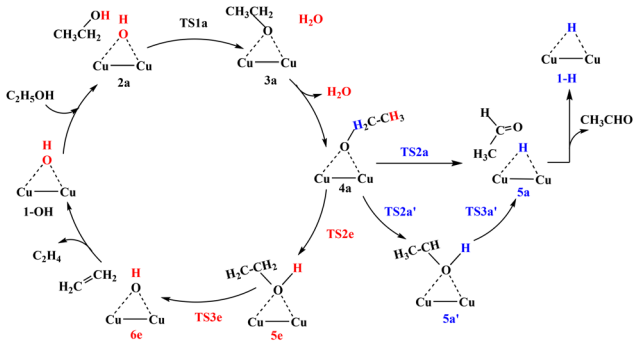

Fig. 5 Schematic diagram for the proposed pathways of transforming ethanol to acetaldehyde and ethylene over the defective HKUST-1(OH) MOF node. Only the Cu active sites are shown for clarity.

 This journal is © The Royal Society of Chemistry 2025

Published on 17 February 2025. Downloaded on 3/19/2026 2:11:47 PM.

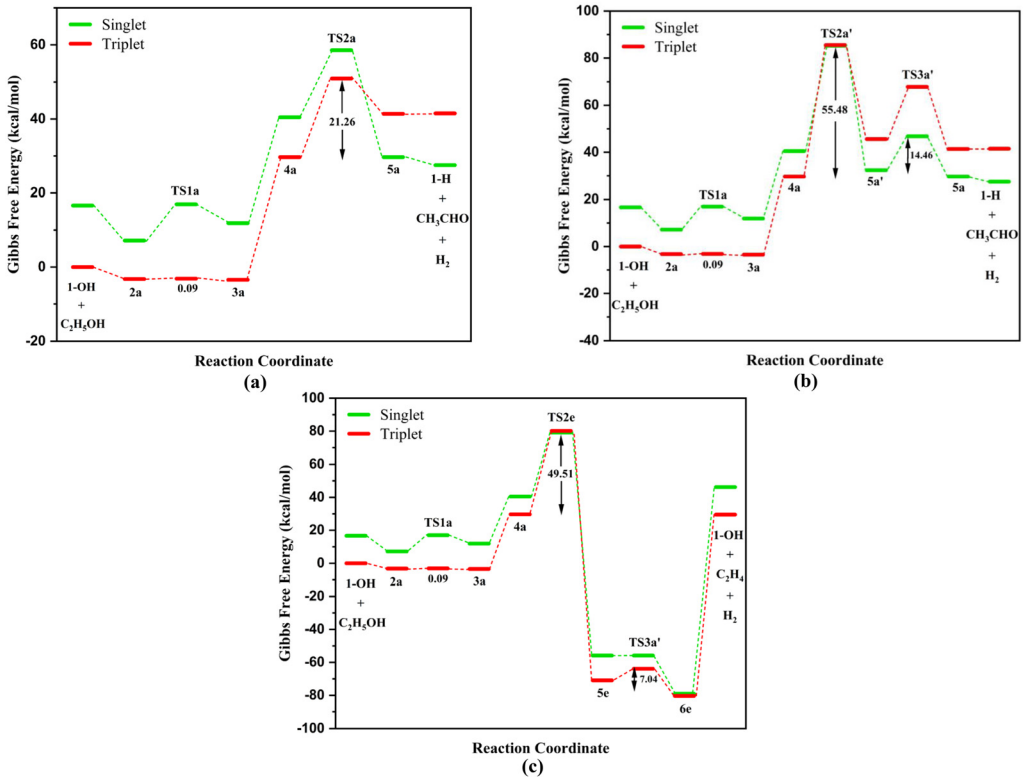

Fig. 6 The reaction profile of acetaldehyde formation from ethanol *via* (a) path-a and (b) path-b, and (c) ethylene formation, over the defective HKUST-1(OH) MOF node. All energies are reported relative to the separated state of catalyst and reactant.

3.4. Catalyst transfiguration

A schematic diagram of the entire picture is presented in Fig. 7. A common phenomenon evident in both HKUST-1(H) and HKUST-1(OH) is the inability of HKUST-1(H) to regenerate the catalyst while following the ethylene formation pathway and the inability of HKUST-1(OH) to regenerate the catalyst while following the acetaldehyde formation pathway. This phenomena did not concern us too much for HKUST-1(H) because we are primarily concerned with acetaldehyde formation and HKUST-1(H) can selectively dehydrogenate ethanol to acetaldehyde while regenerating the catalyst. However, the inability of HKUST-1(OH) to regenerate the catalyst does not prevent it from following the acetaldehyde formation pathway. At a first glance, we might be tempted to name this phenomena as 'catalyst poisoning'. However, a consideration of the complete picture would debar us from doing so. Even though, HKUST-1(OH) gets transformed into HKUST-1(H) while following the acetaldehyde formation pathway, this does not stop the catalytic pathway from going beyond the first cycle. This is because HKUST-1(H) holds the potential to selectively transform ethanol to acetaldehyde. Apparently what seems to be a phenomena of catalyst poisoning, is actually a phenomena of '*catalyst transfiguration*' where the catalyst (HKUST-1(OH)), although transfigured (to HKUST-1(H)), retains its ability to catalyse the reaction. In the first place, one could have easily considered HKUST-1(OH) to be unsuitable for this catalytic transformation. However, on second thought, it becomes immediately evident that catalyst transfiguration does not cause acetaldehyde formation to come to a halt. Even if we had started with HKUST-1(OH), acetaldehyde formation would have been selectively preferred over ethylene formation.

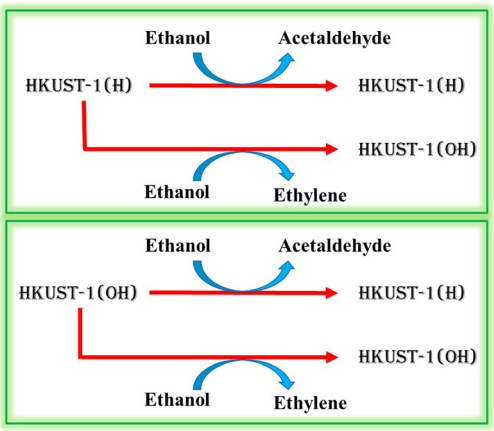

Fig. 7 Schematic diagram representing catalyst transformation of HKUST-1(H) and HKUST-1(OH) MOF nodes.

Published on 17 February 2025. Downloaded on 3/19/2026 2:11:47 PM.

4. Conclusion

To sum up, in the present study, we have carried out a computational investigation on the role of defect-modulated HKUST-1 MOFs (in the form of HKUST-1(H) and HKUST-1 (OH)) in the non-oxidative ethanol dehydrogenation reaction. Inspection of the MOF node structure reveals that the defect free HKUST-1 node is unsuitable for non-oxidative ethanol dehydrogenation and defect modulation in HKUST-1 can provide a way for simultaneous utilization of CUS. It was found that ethanol dehydrogenation to acetaldehyde is preferred over ethylene formation over both HKUST-1(H) and HKUST-1(OH). Although HKUST-1(H) can regenerate itself at the end of the acetaldehyde formation pathway, HKUST-1(OH) cannot; HKUST-1(OH) has been found to transform to HKUST-1(H). We refer to this phenomenon as 'catalyst transfiguration' where the catalyst, although transfigured, retains its ability to catalyse the reaction. In the first place, one could have easily considered HKUST-1(OH) to be unsuitable for this catalytic transformation. However, on second thought, it becomes immediately evident that catalyst transfiguration does not cause acetaldehyde formation to come to a halt. Hence, we can conclude that both HKUST-1(H) and HKUST-1 (OH) can be used to selectively transform ethanol to acetaldehyde where HKUST-1(OH) undergoes transfiguration to HKUST-1(H) at the end of the first catalytic cycle.

Since, (1) Cu-based catalysts are well-known for their ability to catalyse the ethanol dehydrogenation reaction and (2) defective HKUST-1 MOFs have been found to be effective in catalysing ethanol dehydrogenation to acetaldehyde, we expect that Cu-MOFs providing a suitable environment around the active sites (in the form of adjacent metal sites and open structure) can act as an efficient catalyst for this transformation.

Author contributions

Anjali Ganai – Conceptualization, computation, result analysis and interpretation, writing original draft. Pranab Sarkar – Conceptualization, methodology, review and editing, funding.

Data availability

The data supporting this article have been included as part of the ESI.†

Conflicts of interest

There are no conflicts to declare.

Acknowledgements

The authors sincerely acknowledge the financial support from CSIR (HRDG), Government of India [sanction no. 01(3886)/21/EMR-II]. P. Sarkar sincerely acknowledges the financial support from UGC-BSR Mid-Career, Government of India [sanction no. F.19-257/2021(BSR)]. A. Ganai sincerely acknowledges CSIR (HRDG), Government of India for providing the SRF-NET Fellowship [sanction no. 09/0202 (13084)/2021-EMR-I].

References

1 F. Jamil, A. Inayat, M. Hussain, P. Akhter, Z. Abideen, C. Ghenai, A. Shanableh and T. M. Abdellatief, *Adv. Energy Sustainability Res.*, 2024, 2400104.
2 G. Dey, R. Jana, S. Saifi, R. Kumar, D. Bhattacharyya, A. Datta, A. Sinha and A. Aijaz, *ACS Nano*, 2023, **17**, 19155–19167.
3 S. A. Rawool, R. Belgamwar, R. Jana, A. Maity, A. Bhumla, N. Yigit, A. Datta, G. Rupprechter and V. Polshettiwar, *Chem. Sci.*, 2021, **12**, 5774–5786.
4 Z. Zhu, L. Yang, C. Ke, G. Fan, L. Yang and F. Li, *Dalton Trans.*, 2021, **50**, 2616–2626.
5 M. K. Awasthi, S. Sarsaiya, A. Patel, A. Juneja, R. P. Singh, B. Yan, S. K. Awasthi, A. Jain, T. Liu, Y. Duan, *et al.*, *Renewable Sustainable Energy Rev.*, 2020, **127**, 109876.
6 W. Deng, Q. Zhang and Y. Wang, *Dalton Trans.*, 2012, **41**, 9817–9831.
7 M. Moliner, *Dalton Trans.*, 2014, **43**, 4197–4208.
8 F. J. Sama, R. A. Doyle, B. M. Kariuki, N. E. Pridmore, H. A. Sparkes, R. L. Wingad and D. F. Wass, *Dalton Trans.*, 2024, **53**, 8005–8010.
9 T. Pokorny, V. Vykoukal, P. Machac, Z. Moravec, N. Scotti, P. Roupcova, K. Karaskova and A. Styskalik, *ACS Sustainable Chem. Eng.*, 2023, **11**, 10980–10992.
10 R. Pulikkal Thumbayil, D. B. Christensen, J. Mielby and S. Kegnæs, *ChemCatChem*, 2020, **12**, 5644–5655.
11 K. Gao, J. Mielby and S. Kegnæs, *Catal. Today*, 2022, **405**, 144–151.
12 G. Garbarino, P. Riani, M. V. García, E. Finocchio, V. S. Escribano and G. Busca, *Catal. Today*, 2020, **354**, 167–175.
13 L. Lin, P. Cao, J. Pang, Z. Wang, Q. Jiang, Y. Su, R. Chen, Z. Wu, M. Zheng and W. Luo, *J. Catal.*, 2022, **413**, 565–574.
14 M. M. Mohammed, N. S. M. Ali, H. A. Alalwan, A. H. Alminshid and H. A. Aljaafari, *Results Chem.*, 2021, **3**, 100249.
15 Q. Wang, T. Goetjen, J. Hupp, J. Notestein, *et al.*, *J. Catal.*, 2023, **422**, 86–98.
16 V. Paluka, T. Maihom, M. Probst and J. Limtrakul, *Phys. Chem. Chem. Phys.*, 2020, **22**, 13622–13628.
17 J. Pang, M. Zheng, C. Wang, X. Yang, H. Liu, X. Liu, J. Sun, Y. Wang and T. Zhang, *ACS Catal.*, 2020, **10**, 13624–13629.
18 F. Tang, W.-C. Li, D. Wang and A.-H. Lu, *J. Phys. Chem. C*, 2023, **127**, 11014–11025.
19 D. A. Patel, G. Giannakakis, G. Yan, H. T. Ngan, P. Yu, R. T. Hannagan, P. L. Kress, J. Shan, P. Deshlahra, P. Sautet, *et al.*, *ACS Catal.*, 2023, **13**, 4290–4303.

 This journal is © The Royal Society of Chemistry 2025

Published on 17 February 2025. Downloaded on 3/19/2026 2:11:47 PM.

20 S. Hanukovich, A. Dang and P. Christopher, *ACS Catal.*, 2019, **9**, 3537–3550.
21 Y. Huang, B. Wang, H. Yuan, Y. Sun, D. Yang, X. Cui and F. Shi, *Catal. Sci. Technol.*, 2021, **11**, 1652–1664.
22 Q. Wan, F. Wei, Y. Wang, F. Wang, L. Zhou, S. Lin, D. Xie and H. Guo, *Nanoscale*, 2018, **10**, 17893–17901.
23 E. A. Redina, A. A. Greish, I. V. Mishin, G. I. Kapustin, O. P. Tkachenko, O. A. Kirichenko and L. M. Kustov, *Catal. Today*, 2015, **241**, 246–254.
24 Y.-J. Tu and Y.-W. Chen, *Ind. Eng. Chem. Res.*, 2001, **40**, 5889–5893.
25 G. Giannakakis, P. Kress, K. Duanmu, H. T. Ngan, G. Yan, A. S. Hoffman, Z. Qi, A. Trimpalis, L. Annamalai, M. Ouyang, *et al.*, *J. Am. Chem. Soc.*, 2021, **143**, 21567–21579.
26 X. Wang, L. Xu, C. Li, C. Zhang, H. Yao, R. Xu, P. Cui, X. Zheng, M. Gu, J. Lee, *et al.*, *Nat. Commun.*, 2023, **14**, 7210.
27 Y. Li, Y. Li, H. Sun, L. Gao, X. Jin, Y. Li, Z. Lv, L. Xu, W. Liu and X. Sun, *Nano-Micro Lett.*, 2024, **16**, 139.
28 S. S.-Y. Chui, S. M.-F. Lo, J. P. Charmant, A. G. Orpen and I. D. Williams, *Science*, 1999, **283**, 1148–1150.
29 T. Zelenka, M. Balavz, M. Ferova, P. Diko, J. Bednarvcik, A. Kiralyova, L. Zauvska, R. Burevs, P. Sharda, N. Kiraly, *et al.*, *Sci. Rep.*, 2024, **14**, 15386.
30 C. Prestipino, L. Regli, J. G. Vitillo, F. Bonino, A. Damin, C. Lamberti, A. Zecchina, P. Solari, K. Kongshaug and S. Bordiga, *Chem. Mater.*, 2006, **18**, 1337–1346.
31 Y. Wu, Z. Lv, X. Zhou, J. Peng, Y. Tang and Z. Li, *Chem. Eng. J.*, 2019, **355**, 815–821.
32 K.-S. Lin, A. K. Adhikari, C.-N. Ku, C.-L. Chiang and H. Kuo, *Int. J. Hydrogen Energy*, 2012, **37**, 13865–13871.
33 R. Giovine, F. Pourpoint, S. Duval, O. Lafon, J.-P. Amoureux, T. Loiseau and C. Volkringer, *Cryst. Growth Des.*, 2018, **18**, 6681–6693.
34 F. Vermoortele, B. Bueken, G. Le Bars, B. Van de Voorde, M. Vandichel, K. Houthoofd, A. Vimont, M. Daturi, M. Waroquier, V. Van Speybroeck, *et al.*, *J. Am. Chem. Soc.*, 2013, **135**, 11465–11468.
35 Y. Liu, R. C. Klet, J. T. Hupp and O. Farha, *Chem. Commun.*, 2016, **52**, 7806–7809.
36 C.-L. Zhang, T. Zhou, Y.-Q. Li, X. Lu, Y.-B. Guan, Y.-C. Cao and G.-P. Cao, *Small*, 2023, **19**, 2205898.
37 W. Zhang, M. Kauer, P. Guo, S. Kunze, S. Cwik, M. Muhler, Y. Wang, K. Epp, G. Kieslich and R. A. Fischer, *Eur. J. Inorg. Chem.*, 2017, **2017**, 925–931.
38 Y. Injongkol, T. Maihom, S. Choomwattana, B. Boekfa and J. Limtrakul, *RSC Adv.*, 2017, **7**, 38052–38058.
39 W. Jeevapong, J. Sittiwong, M. Probst, B. Boekfa, C. Wattanakit, T. Maihom and J. Limtrakul, *J. Phys. Chem. C*, 2023, **127**, 8473–8481.
40 K. Hashem, R. Krishnan, K. Yang, B. A. Anjali, Y. Zhang and J. Jiang, *Phys. Chem. Chem. Phys.*, 2024, **26**, 7109–7123.
41 I. Agirrezabal-Telleria, I. Luz, M. A. Ortuño, M. Oregui-Bengoechea, I. Gandarias, N. López, M. A. Lail and M. Soukri, *Nat. Commun.*, 2019, **10**, 2076.
42 W. Xue, J. Wang, H. Huang, Y. Cui and D. Mei, *J. Phys. Chem. C*, 2022, **126**, 9652–9664.
43 J. Frenzel, J.-O. Joswig, P. Sarkar, G. Seifert and M. Springborg, *Eur. J. Inorg. Chem.*, 2005, **2005**, 3585–3596.
44 B. Goswami, S. Pal and P. Sarkar, *Phys. Rev. B: Condens. Matter Mater. Phys.*, 2007, **76**, 045323.
45 M. J. Frisch, G. W. Trucks, H. B. Schlegel, G. E. Scuseria, M. A. Robb, J. R. Cheeseman, G. Scalmani, V. Barone, G. A. Petersson, H. Nakatsuji, X. Li, M. Caricato, A. V. Marenich, J. Bloino, B. G. Janesko, R. Gomperts, B. Mennucci, H. P. Hratchian, J. V. Ortiz, A. F. Izmaylov, J. L. Sonnenberg, D. Williams-Young, F. Ding, F. Lipparini, F. Egidi, J. Goings, B. Peng, A. Petrone, T. Henderson, D. Ranasinghe, V. G. Zakrzewski, J. Gao, N. Rega, G. Zheng, W. Liang, M. Hada, M. Ehara, K. Toyota, R. Fukuda, J. Hasegawa, M. Ishida, T. Nakajima, Y. Honda, O. Kitao, H. Nakai, T. Vreven, K. Throssell, J. A. Montgomery Jr., J. E. Peralta, F. Ogliaro, M. J. Bearpark, J. J. Heyd, E. N. Brothers, K. N. Kudin, V. N. Staroverov, T. A. Keith, R. Kobayashi, J. Normand, K. Raghavachari, A. P. Rendell, J. C. Burant, S. S. Iyengar, J. Tomasi, M. Cossi, J. M. Millam, M. Klene, C. Adamo, R. Cammi, J. W. Ochterski, R. L. Martin, K. Morokuma, O. Farkas, J. B. Foresman and D. J. Fox, *Gaussian~16 Revision C.01*, Gaussian Inc., Wallingford CT, 2016.
46 J. Ye, L. Gagliardi, C. J. Cramer and D. G. Truhlar, *J. Catal.*, 2018, **360**, 160–167.
47 W. Xue, X. Song and D. Mei, *J. Phys. Chem. C*, 2021, **125**, 17097–17108.